Adaptive and Wireless Recordings of Electrophysiological Signals during Concurrent Magnetic Resonance Imaging

Ranajay Mandal, Nishant Babaria, Jiayue Cao and Zhongming Liu*, *Senior Member IEEE*

***Abstract*—Strong electromagnetic fields during functional magnetic resonance imaging (fMRI) presents a challenging environment for any concurrent electrophysiological recording. Here, we present a miniaturized, wireless platform – "MR-Link" (Multimodal Recording Link) that provides a hardware solution for simultaneous electrophysiological and fMRI signal acquisition. The device detects changes in the electromagnetic field during fMRI and synchronizes amplification and sampling of electrophysiological signals to minimize effects of gradient and RF artifacts. It wirelessly transmits the recorded data at a frequency detectable by the MR-receiver coil. The transmitted data is readily separable from MRI in the frequency domain. To demonstrate its efficacy, we used this device to record electrocardiograms and somatosensory evoked potential without artifacts from concurrent fMRI scans, or compromising imaging quality. The compact recording device (20 mm dia., 2gms) placed within the MR-bore minimized movement artifacts and achieved microsecond-level synchronization with fMRI data. MR-Link offers an inexpensive system to eliminate the need for amplifiers with high dynamic range or sampling rate, high-power sampling, additional storage or synchronization hardware to connect with the MR-scanner. This device is expected to enable easier and a broader range of applications of simultaneous fMRI and electrophysiology in animals and humans.**

***Index Terms*— Simultaneous fMRI-EEG, Wireless, frequency modulation, gradient artifacts**

I. Introduction

Simultaneous acquisition of functional magnetic resonance imaging (fMRI) in combination with electroencephalography (EEG), electrocorticography (ECoG), local field potentials (LFP), and single or multi-unit activity (SUA/MUA) holds great potential to bridge neural activity across spatial and temporal scales [1]–[11]. Despite its scientific premise and clinical potential, concurrent electrophysiological (EP) and MRI acquisition is challenging, as the MRI apparatus presents a hostile environment for recording bioelectric signals [3], [6], [9], [12]. MR-safety and compatibility are the first and paramount concern for any recording device working inside MRI. Apart from safety, the major bottleneck is the electromagnetic (EM) artifacts generated by (a) the static magnetic field, (b) strong RF deposition, and most importantly (c) rapidly changing gradient magnetic fields [7], [13]–[15]. These artifacts may be several orders of magnitude larger than the signals of interest. As a result, the recorded EP data is often unusable to researchers without specialized technical expertise.

The most widely used method of EM artifact removal for recovery of the EP signals of interest, involves rigorous offline post-processing of the artifact-corrupted dataset [3], [16], [17]. Since these artifacts are considerably larger in magnitude than the signals of interest, all commercially-available recording systems use high-power amplifiers with a large dynamic range and a high sampling rate (>5KHz) [16], [18]. Such amplifiers are often used along with additional shielding and powering modules, making the whole system complex, bulky, expensive, and of significant safety concern, especially in high-field MRI [15]. Moreover, retrospective artifact removal is technically demanding even if the artifacts and signals are recorded with high fidelity. Signal processing algorithms for artifact correction have been getting increasingly sophisticated [19]–[22]. However, their efficacy is limited, since the artifacts of concern may be non-stationary or inter-mixed with other types of noise (e.g. head motion) and thus difficult to isolate or remove [12], [16], [19]–[23]. Even a relatively small percentage of residual artifacts can be very problematic for recovering weak signals such as EEG [20].

In this regard, several interesting approaches have been proposed to prevent EM artifacts from corrupting EP recordings. For example, Anami et al. have proposed a so-called "stepping stone sampling" strategy to skip the EM artifact by selectively sampling EEG only during the "silent" period of MRI [13]. This strategy requires the synchronization of the operational clocks of the MR scanner and the EEG system, presumption on the MRI pulse sequence, and triggered 20 kHz sampling, all of which place a considerable level of complexity to the recording system, and limit the scope of application [13]. In addition, Hanson et al. have proposed a complementary strategy to wirelessly transmit EP recordings for reception by the MRI receiver coil, while utilizing the surplus hardware in the MRI system [24]. While considerable

This work was supported in part by NIH R01MH104402, Purdue Research Foundation and Purdue University. Authors have no conflict of interest. *Asterisk indicates corresponding authors.*

Ranajay Mandal and Jiayue Cao are with the Weldon School of Biomedical Engineering and Purdue Institute for Integrative Neuroscience, Purdue University, West Lafayette, IN, USA.

Nishant Babaria is with the School of Electrical and Computer Engineering, Purdue University, West Lafayette, IN, USA.

*Zhongming Liu is with the Weldon School of Biomedical Engineering, School of Electrical and Computer Engineering, and Purdue Institute for Integrative Neuroscience, Purdue University, West Lafayette, IN, USA. (correspondence e-mail: zmliu@purdue.edu).

reduction of gradient artifacts was observed, additional post-processing effort was necessary to remove cross talks between "MR" and "Non-MR" data. Furthermore, the comparatively bulky system (2 kg), operated from outside the MR-bore, required long wired connections to carry out the EP data. Thus, the advantages of the proposed method are further compromised as it fails to mitigate major concerns about movement related artifacts.

These circumstances necessitate a simpler and more robust method for integrating EM-artifact-free multimodal imaging (or any biopotential) data alongside conventional fMRI data. Utilizing the special characteristics of these artifacts and surplus MR-hardware, we developed an MR-integrated, wireless method and a miniaturized platform, "MR-Link" (Multimodal Recording Link) for high-fidelity EP acquisition during simultaneous fMRI (Figure 1). The device contained on-board coils and analog/digital circuits to be able to detect the timing of gradient changes, and accordingly amplify and sample EP signals to prevent gradient artifacts from corrupting the EP signals. It also contained an onboard transmitter to send the recorded EP signals to the MRI receiver coil without interfering with MRI acquisition. As such, the device could operate locally and wirelessly, increasing the signal to noise ratio while reducing the EM and movement artifacts that would otherwise occur to typically wired recording systems [15]. It facilitates the use of MRI scanner for both imaging and recording through its existing hardware. Hereafter, we describe the system design and implementation, alongside a series of experimental EP (ECG, LFP and SEP) recordings to demonstrate the efficacy and potential of this device.

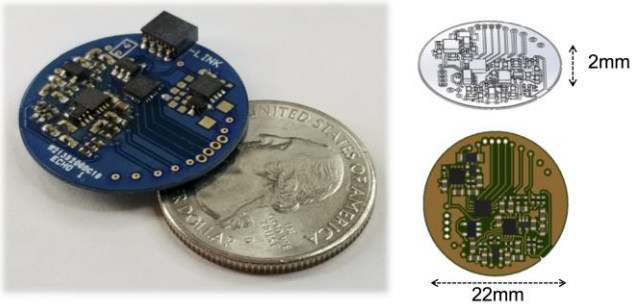

Fig. 1. MR-Link Recorder (Right) and CAD representation (Left) depicting the miniaturized size of the device.

II. Materials and Methods

A. Device Overview

The device was designed to utilize the existing MRI hardware and the EM environment in the MRI system to trigger EP recording and transmit digitized data. The device recorded the EP signal based on the input it received from the gradient detection system which monitored changes in the magnetic field inside the MRI bore [25]. The device amplified and filtered the EP signal, and transmitted it wirelessly to the MR-receiver coil during MRI acquisition. The EP and MR signals were modulated by different frequencies such that they could be separated and demodulated without mutual interference (Figure 2). Figure 3 illustrates the major components of the device. Each of these components are described in the following subsections.

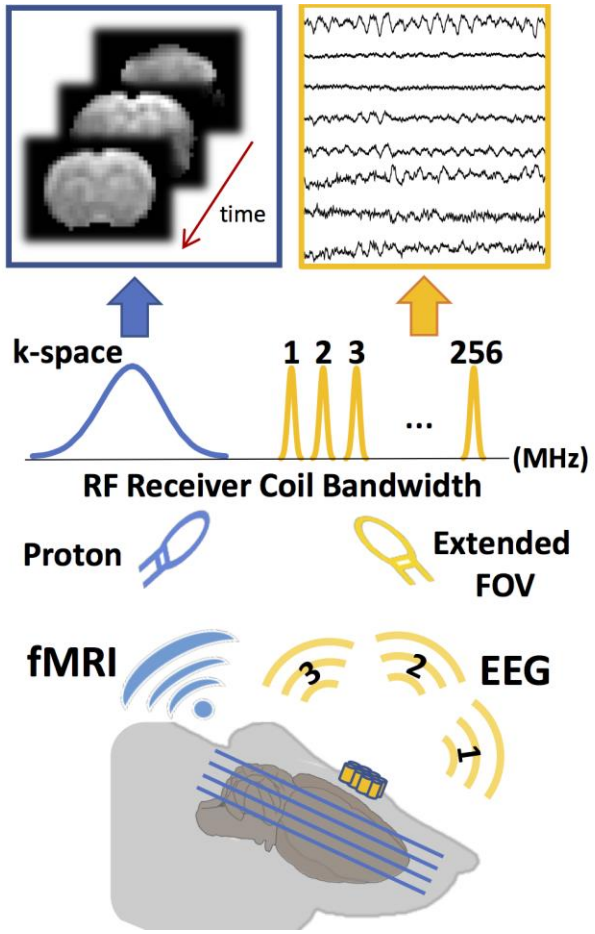

Fig. 2. Concurrent fMRI and EP signal recording utilizing MR-receive coil. Amplified and digitized EP data is modulated by the MR-link recorder at discrete frequencies, visible to the MR-receiver coil. RF echo from the subject is sensed by the receiver coil near the center frequency of MRI scanner (Blue). Simultaneously, the EP data, modulated with an offset (w.r.t the MRI center frequency) is also detected (Yellow). This spectrally isolated EP data becomes embedded into the extended FOV of the reconstructed MR image.

B. Gradient detection circuit

The gradient detection circuit utilized a machine-wound copper coil to pick up variations in the magnetic field inside the MRI bore. The differential signal from the coil was passed through a voltage limiter and rectifier circuit before being filtered through a single-stage low-pass filter (fc = 30kHz) (Figure 3(d)). The filter removed high frequency signal components while retaining the RF envelope for detection. A comparator was lastly used to generate a negative logic binary output (hereafter referred to as the gradient trigger), reporting whether the magnetic field was static (1) or varying (0), respectively. The gradient trigger was then fed into a microcontroller (µC) which managed the onboard operations of the device discussed hereafter.

C. Adaptive Sampling

The gradient detection circuit made it possible to sample EP signals at discrete points in time to avoid gradient and RF artifacts [13]. The onboard µC sampled the analog EP signal using its 10-bit analog to digital converter (ADC). ADC sampling was only initiated when the gradient trigger was high

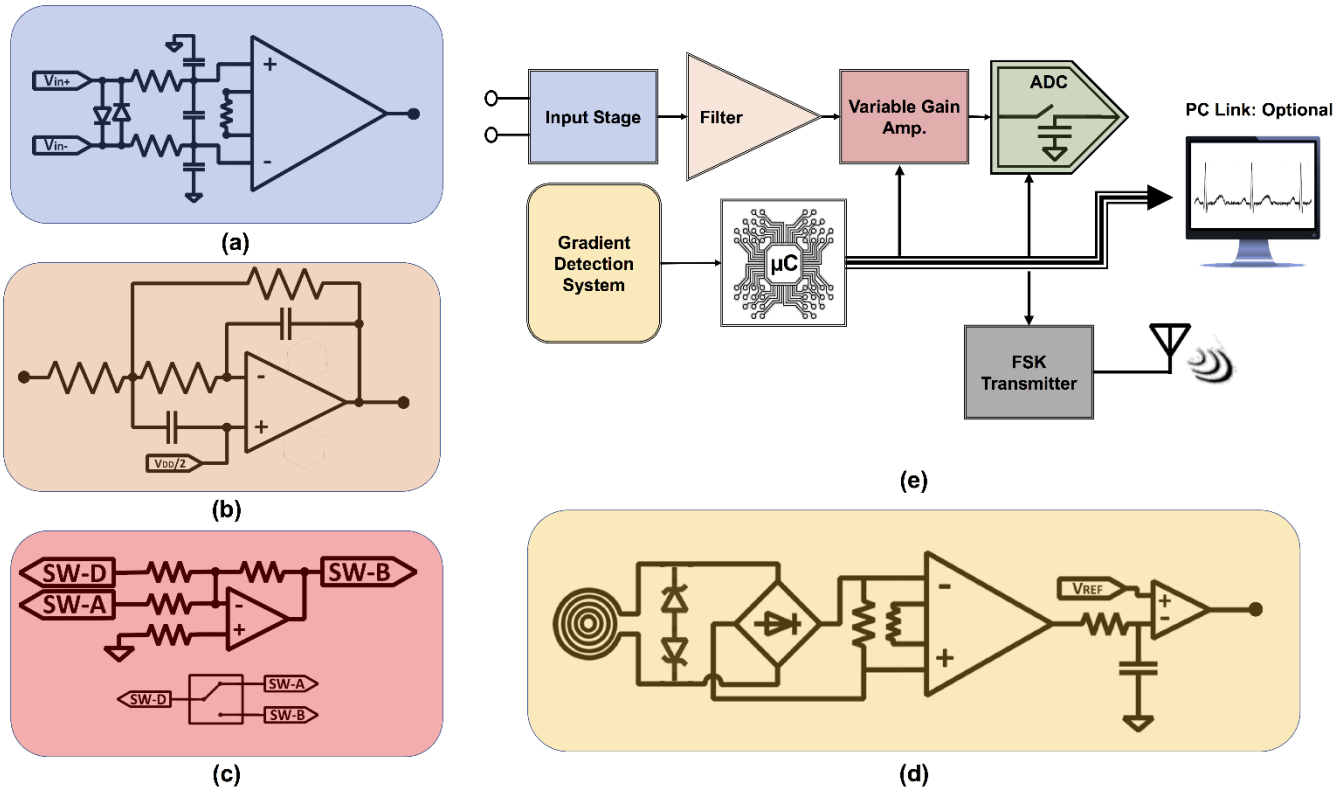

Fig. 3. Simplified MR-Link Recroder circuit schematic. The EP signal is processed by the variable gain (c), analog filtering circuit (a,b) and subsequently digitized through the microcontroller (e). Variable again and digitization are triggered by the gradient detection circuit(d). Digitized data is transmitted wirelessly through a low-power UHF transmitter. Alternatively, the data can also be accessed through an USB PC-link. (a) Input differential stage with a low-pass filter (15 KHz) and gain of 6.02 dB. (b) Second order low-pass filter (15 KHz) with a gain of 0 dB. (c) Gain switching stage with gain of 54 dB during 'plateau period' and attenuation of -54 dB during 'ramping period' of the gradient. (d) Gradient detection circuit which monitors the electromagnetic field changes inside the MRI bore through a machine wound coil (14mm dia.) and outputs a binary signal to denoting the presence of gradient and RF artifacts.

and was further regulated by a pattern learning feature (adaptive sampling) programmed onto the µC. The basic premise of the µC code was to initiate EP sampling and transmission during periods without gradient pulses, or in other words, when the MRI was receiving RF echoes from the subject (Figure 4).

The adaptive sampling microcode monitored the time periods of the gradient trigger and used this information to regulate device operations. µC timers and their associated interrupts were utilized to build the backbones of adaptive sampling and gave it functionality to monitor time. The duration of µC operations such as ADC sampling and UART communication were a function of the µC clock frequency and were thus constant once the µC was initialized. These constant times of each device operation were experimentally profiled at 1MHz clock frequency and were provided as constants in the adaptive sampling routine. Thus, with the knowledge of the duration of plateau periods and each operation, the device µC can alter its configuration to complete sampling, gain switching, and wireless data transmission within the plateau regions.

D. Analog filtering and amplification

The analog filtering and amplification system (or the analog circuit) on the device consisted of two variable gain amplifiers (VGA), which were assisted by a passive differential low-pass filter and another second-order active low-pass filter. Additionally, a voltage limiter circuit, like that used in the gradient detection system, was incorporated at the input stage to limit the amplitude of the gradient artifacts (Figure 3(a)). The main operation of the analog circuit was to attenuate the incoming signal when the gradient trigger was low and to provide amplification when the gradient trigger was high. This assured that the analog system did not saturate due to the strong gradient artifacts.

The low-pass filters were both cutoff at 15kHz to reject any high-frequency EM interference, while providing a sufficient bandwidth to capture a wide range of EP signals. The discrete-time variable-gain amplification was essential to avoiding gradient artifacts, the timing of which was predicted in real-time by the gradient detection circuit. The two VGAs individually provided +/- 27 dB based on the information provided by the gradient trigger. The maximum gain applied to the EP signal was 60 dB during the readout period (gradient plateau) and conversely, the maximum attenuation applied was -54 dB during the ramping periods. Apart from the VGAs, 6 dB of constant gain was provided by the instrumentation amplifier at the input stage, where the differential EP signal was converted to a single-ended signal for filtering and further processing by the VGAs (Figure 3(c)).

E. Wireless Transmission

The digitized packets were wirelessly transmitted through a low power ultra-high frequency (UHF) transmitter using binary Frequency Shift Keying (FSK). The carrier frequency of the RF signal was programmed within the bandwidth of the MR-

receiver coil, but outside of the frequency range for MR signal reception [24]. The transmission power, carrier frequency (300.043MHz), deviation frequency (9.6KHz), data modulation types (FSK) and data rate (19.2Kbps) were all programmed and controlled through the µC. The built in fractional-N PLL (Phase-locked loop) of the transmitter was utilized for narrow-band operation. The reference frequency was generated through a crystal oscillator with a frequency tolerance and temperature stability of 10 ppm. Furthermore, frequency error in crystal reference were compensated indirectly through an inbuilt compensation register so that the output can be varied at <1 ppm steps. The output power of the transmitter was programmed from -16dBm to +14dBm with 0.4dBm steps. A fifth order Chebyshev filter, placed at the output of the transmitter ensured attenuation of third and fifth order harmonics.

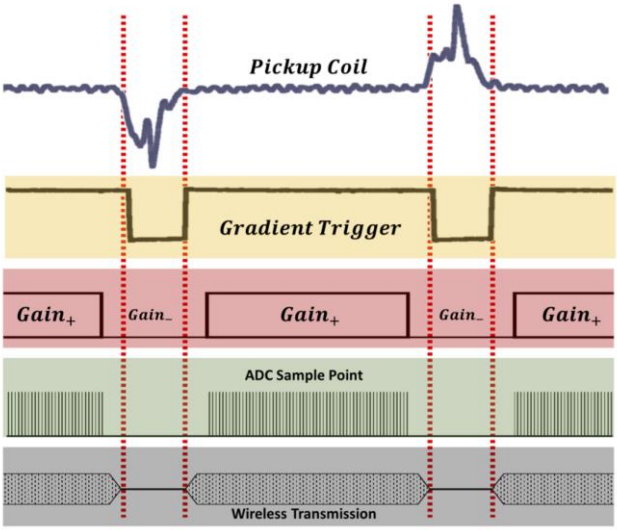

Fig. 4. Gain switching, adaptive sampling, and data transmission driven by the gradient detection circuit. Pickup coil signal is translated into the binary gradient output which allows the onboard microcontroller to modulate gain and sample EP signal to avoid MR artifacts (Row 1-4). Digitized data is transmitted (wirelessly or wired) during 'plateau period' (Row 5).

F. FOV extension for EP reception

The FOV for imaging was extended along the readout direction to allow RF-modulated EP data to be received by the MR-receiver coil. The image matrix along the readout direction contained 256 points. The receiver bandwidth was set to 333.333KHz to provide sufficient sampling rate for implementing FSK modulation of transmitted data. During each of the K-space line scans while the receive coil was 'ON' (set to acquire RF signals), digitized EP data was transmitted from the device (Figure 5). This triggering was again done through the gradient detection unit. As a result, the non-MR data was automatically synchronized with the fMRI images.

Each k-space line acquisition duration was 600us along with two ramp up and ramp down periods of 100us each. During the plateau region of 600us, 16 samples of EP signal were taken and averaged within the µC. The processed data was then transmitted in the next plateau region. During each slice acquisition 64 EP data points were recorded through the MR-image at a sampling rate of 1.3KHz.

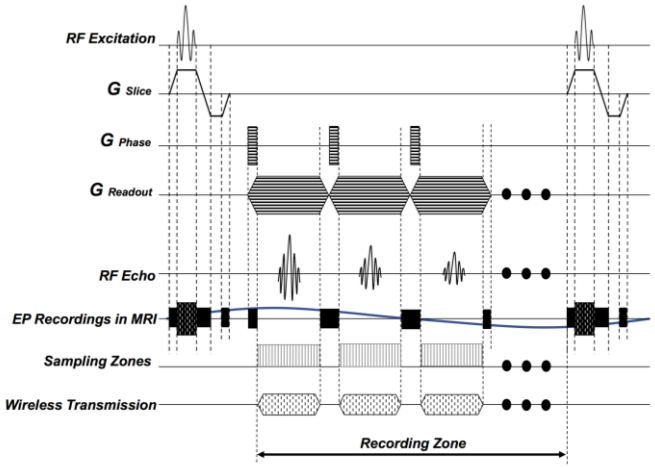

Fig. 4. Gradient and RF pulses, as generated during the echo-planar-imaging (EPI) sequence. The discrete nature of the electromagnetic artifacts and there timings with respect to the gradient and RF pulses are shown on rows 1-6. Rows 7-8 show the sampling and transmission zones associated with the device operation.

G. Data Handling and Post Processing

The transmitted EP signals and the fMRI images were stored conveniently in the same file following DICOM archiving standards. Just after the scans were completed, the RAW data was fed into a custom software, developed using MATLAB (MathWorks, MA, USA). The software isolated the MR-data and non-MR data based on their respective frequency ranges. Furthermore, the software stored the MR data, containing all the imaging information in the file format (i,e. 32-bit, integer etc.) compatible with ParaVision 6.0.1, Bruker Software (BioSpec 70/30, Bruker, MA, USA) for image reconstruction.

The isolated, non-MR data contained wirelessly transmitted EP signal which was already demodulated by the MR-center frequency. The extracted data was comparable to a digitized intermediate frequency (IF) signal, very common in RF receiver system. The scanner acted as a mixer for the FSK modulated data. Firstly, the mark and space frequencies (binary '1' and '0') were identified by calculation of power spectral density (PSD) of the non-MR data set. In the second step, asynchronous or non-coherent demodulation scheme was implemented to retrieve the digital packets (Figure 6). The received signal was treated as a sum of two amplitude shift keyed signals (ASK) and matched filters isolated these two ASK signals. Finally, the binary signal train was recovered through two envelope detectors and a logic synthesizer, all implemented on MATLAB script.

H. Experimental Paradigms

Our current investigation focused primarily on implementation of the proposed method, through phantom imaging (Phantom Study) while EP data recording was carried out by the device. Additionally, efficacy and validation of the MR-Link device as an MR-integrated recording platform was analyzed through simultaneous recording of cardiac and brain evoked response during simultaneous fMRI of a rat. Finally, the effects of the device operation within MR-bore was analyzed qualitatively and quantitatively to further illustrate the advantages of the proposed technique.

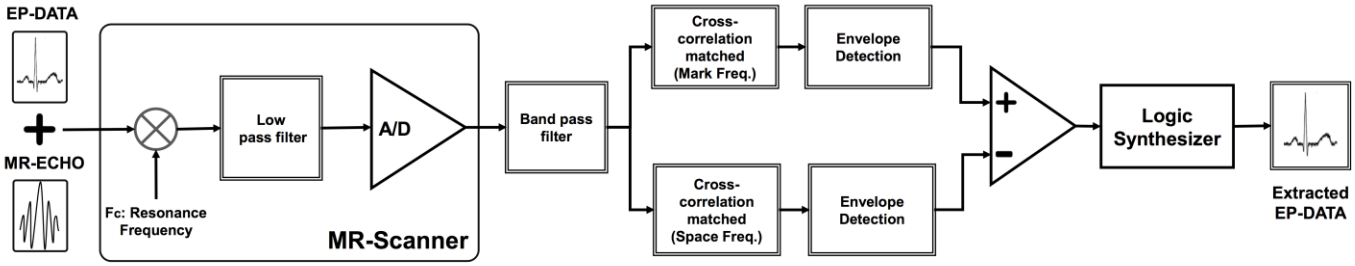

Fig. 6. Block diagram of the wireless EP-data reconstruction method. Both MR-echo and modulated EP signal, sensed by the receiver coil is demodulated at MRI-center frequency (300.033 Mhz) and digitized by the scanner. The raw fMRI data is then bandpass filtered to isolate the non-MR data and standard FSK demodulation scheme was employed to reconstruct the MR-Link device recorded EP data.

I. Subjects and materials

A test tube with $CuSO_4$ x $2H_2O$ (1g/L) solution was used in the phantom study. Albino rat species Rattus norvegicus was utilized in both the in vivo studies specified above. All subjects were healthy males between the ages of 4-8 months. The Ag/AgCl, radiolucent ECG electrodes (NeoTech Products, Inc., CA, USA) were utilized for their MR-compatibility in the ECG study. The neural electrodes used in the in vivo study were manufactured by Plastics One (Plastics One, VA, USA) with the active electrode diameter of 0.127mm and a length of 3mm. The reference electrode was of the same diameter, but its length was 10mm for specific purpose as explained under General surgery description. Both active and reference electrodes were made from platinum (Pt) to be MR-compatible. Additionally, the pedestal of the electrodes and the inner connectors were made of plastic and copper (Cu) respectively to be MR-compatible. To secure the electrode, nylon plastic screws were used. Similar types screws served to provide ground and reference points on the skull. A 0.3mm hole was drilled into the screws through which the ground and reference electrodes could pass and contact the brain. All experiments were conducted using a Brucker animal MRI.

J. Phantom Study

The test tube phantom and the MR-Link recording system were placed inside the MRI while the phantom was imaged using an echo-planar imaging (EPI) sequence (described in MRI Protocol and Pulse Sequence). MR-Link system was primarily supplied with a dummy signal from a function generator to transmit wirelessly and receive through the MRI receiver coil. During the study, the wireless transmitter power and the carrier frequency were also tuned, to avoid any overlap with the imaging data.

The MR-Link system was triggered initially using the gradient signal from the MRI server and later utilizing the gradient detection system to synchronize its transmission. The gradient detection module was evaluated in the phantom study to produce an accurate response to changing magnetic field in the MRI bore. The pick-up coil was placed at 45° angle with respect to the Gx and Gy plane to ensure magnetic variation along the x or y axis were registered by the gradient detection circuit. The coil was secured to the outside of a custom-made animal tray to keep the orientation stable throughout the experiments.

Apart from recording the dummy signal, efficacy of the amplifier system was further verified through the acquisition of neural signals (LFP and SEP) from a rat, placed outside the MR-bore. Local field potentials (LFP) were recorded from right somatosensory cortex (R-S1FL) under two conditions: (a) variation of anesthesia levels and (b) forepaw electrical stimulation (described in General neurosurgery description and fMRI setup).

K. In vivo ECG during fMRI

The in vivo ECG experiment was first conducted to monitor a reliable and well-known bio-signal to validate the device's function inside the MRI [14], [24]. The rat was anesthetized (3% isoflurane in oxygen at 1L/min) and shaved at the site where the electrodes were placed. The electrodes were placed in Einthoven's Triangle formation. The signal was checked with a benchtop Grass Cp511 Amplifier and the device to verify that Echo was functioning properly outside the MRI. The rat was placed inside the MRI in supine position and the electrode leads were pulled out as straight as possible to connect with the device. The device was placed adjacent to the rat at the foot of the animal tray holder. The rat was kept under anesthesia with a continued supply of isoflurane throughout the experiment (2% isoflurane in oxygen at 0.5L/min). The rat breathing rate and SpO_2 levels were constantly monitored with the use of Kent Scientific Rodent Pulse Oximeter (Torrington, USA) and adjustments to the anesthesia were made if needed. The animal tray was also continuously flushed with warm water to act as a heating bed for the animal and help regulate its body temperature. The water temperature was held constant at 40°C.

L. In vivo LFP during fMRI

The in vivo neuro experiment was conducted to monitor evoked potential in the right somatosensory cortex (R-S1FL) of the rat. The rat was prepared for the electrode implant by administering painkiller (carprofen, 5mg/kg) before being anesthetized (3% isoflurane in oxygen at 1L/min). The rat was then shaved at the site of the surgery and placed into a stereotaxic instrument (Stoelting, IL, USA). A continued supply of isoflurane was administered to keep the rat anesthetized for the duration of the procedure (2% isoflurane in oxygen at 0.5L/min). A heating pad with an active body (rectum) temperature feedback was utilized to help regulate the rat's body temperature. All measurements taken to place the electrode were about the bregma. A 1mm hole was drilled into

the skull above the R-S1FL (AP+0.2mm and ML+3.5mm). The Pt electrode was inserted 2.5mm (DV+2.5mm) into the brain before being fixated with dental cement. The ground and reference points were placed in the region above the cerebellum (posterior to the lambda). Nylon plastic screws with holes were placed into the holes for ground and reference. The reference electrode and a separate ground wire were inserted into the screws and then fixated using dental cement. The left forepaw was stimulated using a current stimulator (A-M Systems, WA, USA) (1mA, 5ms, 10Hz, monophasic pulse) to verify the position of the electrode. The benchtop response was recorded and filtered by Grass Cp511 Amplifier and the device for validation outside the MRI.

The rat was placed in the prone position into the MRI after a successful electrode implant. To better induce a clear hemodynamic response in R-S1FL the anesthesia method and dosage were altered for the imaging session (0.03mg/Kg/h dexmedetomidine subcutaneously and 0.2-0.3% isoflurane). The active, reference, and ground wires were pulled straight out and connected to the device. The device placement and the general MRI setup was as described in the ECG study setup section. The rat's vitals were monitored using Kent Scientific Oximeter and the isoflurane was adjusted as needed.

M. Effects on fMRI data quality

Lastly, the effects of wireless transmission on MR-images were quantitatively assessed through analyzing the tSNR characteristics of the EPI image. The EPI image sequence described in pulse sequence was used to acquire a BOLD image while the rat was administered forepaw stimulation. The BOLD response was recorded from rat brain for two sets of experimental conditions. One condition included the MR-Link system operating normally ("ON") and wirelessly transmitting EP data to scanner receiver coil. In the second condition, the MR-Link system was disconnected from its power supply and kept in the "OFF" state. The correlation between forepaw stimulation and the BOLD response was calculated for both conditions and compared. The animal and MRI setup for the study was as described in the General neurosurgery description and fMRI setup.

III. RESULTS

A. Phantom Study

The phantom study outlined a repeatable experimental setup to test the device for in vivo EP recording within the MR-bore. Initially, an ECG signal (3mVpp, 1.2Hz), generated from an arbitrary function generator, was chosen as a sample EP data for this purpose. The sample signal was amplified and digitized through the MR-Link device before being wirelessly transmitted during concurrent imaging of a phantom. The wireless data appeared in the extended FOV of the image as seen by the two white lines in (Figure 7). FOV extension along the readout direction increased the image width and accommodated the non-MR data effectively without any overlap with the phantom image. The image reconstruction was done once more through the scanner console after non-MR data was filtered out using the custom software. The MATLAB based extraction software successfully reconstructed the sample data and relatively high SNR was observed. Various distinct waves (P, Q, R, S, and T) are clearly visible in the extracted ECG signal which was generated using a function generator (Figure 7).

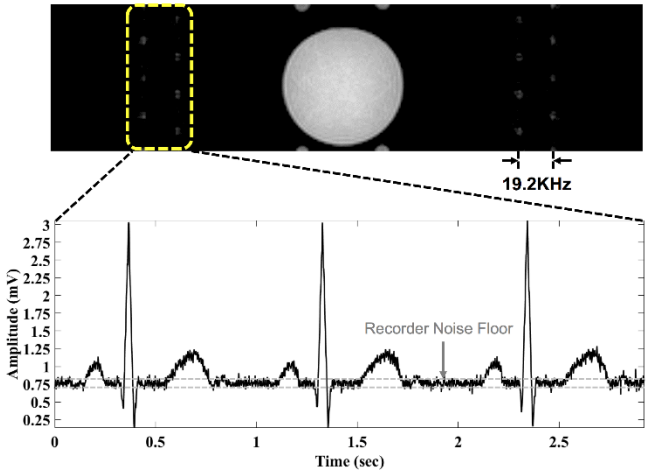

Fig. 7. Phantom image with simulated ECG signal embedded into the FOV of MR image. The FSK modulated (BW 19.2Khz) ECG data appear as lines in the extended FOV. The EP data reconstructed from the fMRI image sequence is shown below.

Furthermore, LFP and SEP signals were recorded from rat S1FL using the device setup while the animal was placed outside the MRI. The recorded LFP varied with the level of anesthesia and as isoflurane concentration was varied to induce deeper anesthesia, the LFP signals showed characteristics of burst suppression (Figure 8). Furthermore, somatosensory evoked potential due to a forepaw current stimulus (1mA, 5ms, 10Hz) was clearly picked up by the device at a high SNR (Figure 8). The SEP varied with frequency, current amplitude and pulse width durations.

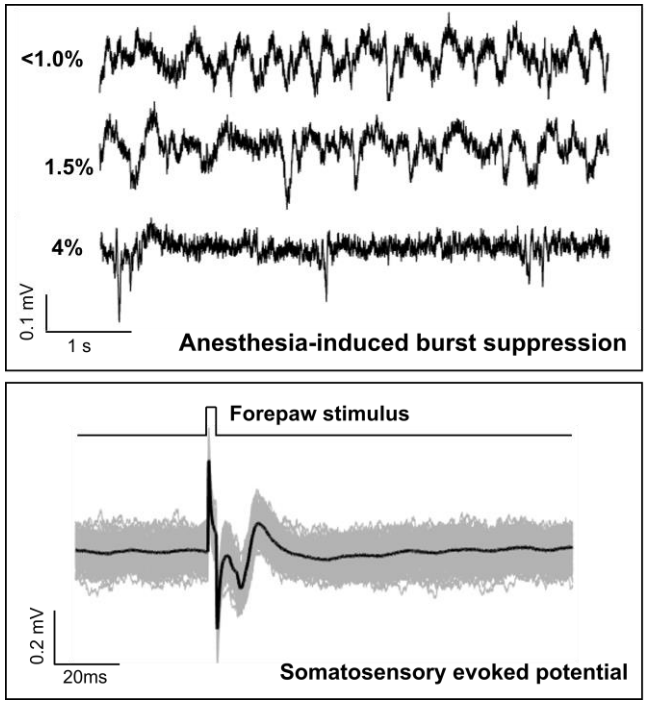

Fig. 8. Rat LFP observed with active sensing outside the MR-bore. Somatosensory evoked potential due to forepaw stimulus (Top).Spontaneous LFP changed progressively with deeper anesthesia (isoflurane concentration) towards burst suppression(Bottom).

B. *Cardiac Signal recording during simultaneous fMRI*

In vivo ECG signal was recorded from a rat placed inside the MR-bore while image slices were taken surrounding the brain region. For cross validation of the data extraction technique, digitized data was recorded using two methods simultaneously: (a) the MR-receiver coil during imaging and (b) digital UART-USB link on a custom software. The device effectively rejected any gradient artifacts and the cardiac signals, extracted from the MR-images, required no further postprocessing. Furthermore, as visible from Figure 9, the ECG data was inherently synchronized and time stamped with corresponding brain slices. Additionally, magneto-hydrodynamic effect due to the presence of strong static magnetic field (7T) was also observed as the T waves were significantly enlarged [14].

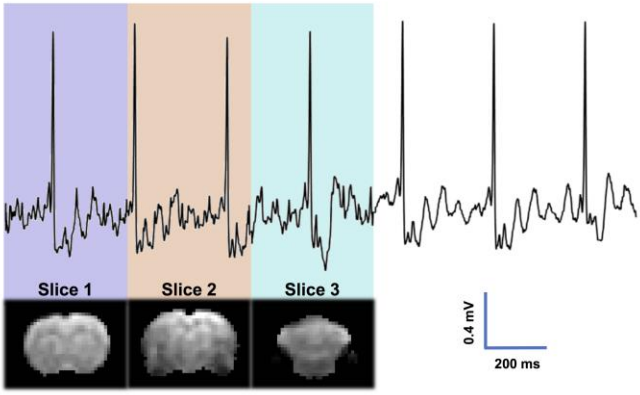

Fig. 9. Synchronization of the recorded rat ECG and with corresponding fMRI image slice. ECG data acquired at a sampling frequency of 1.3Khz except during inter-slice 'blip' zones (~5ms).

C. *Evoked potential recording during simultaneous fMRI*

The MR-Link system successfully recorded in vivo evoked potential from right somatosensory cortex due to electrical stimulation of forepaw, as seen in Figure 10. The evoked response data was reconstructed and correlated with the stimulation trigger to delineate the onset of the stimulation and the response which followed the paradigm shown in Figure 11. To evaluate the efficacy of the multimodal data acquisition method, simultaneous functional imaging was carried out. Somatosensory evoked potential, when correlated with fMRI images to show BOLD response centered at R-S1FL (Figure 10). The evoked response study clearly establishes the significance of the proposed method as a simple and effective solution for simultaneous neural-imaging and recording.

D. *Effects on fMRI data quality*

A systematic experimental paradigm was designed to evaluate the effect of wireless transmission on the MR-images (Figure 11). The correlation map between the forepaw stimulation and the BOLD response was analyzed for the "ON" and "OFF" states. As the device transmitted EP signals in frequencies visible to the receiver coil, it was imperative to observe whether these additional non-MR signals affected the quality of BOLD signals, derived from the MR-signals. The BOLD response map in both the conditions showed a very similar profile and thus depicting qualitatively that there was no effect of MR-Link transmitter on MRI diagnostic environment

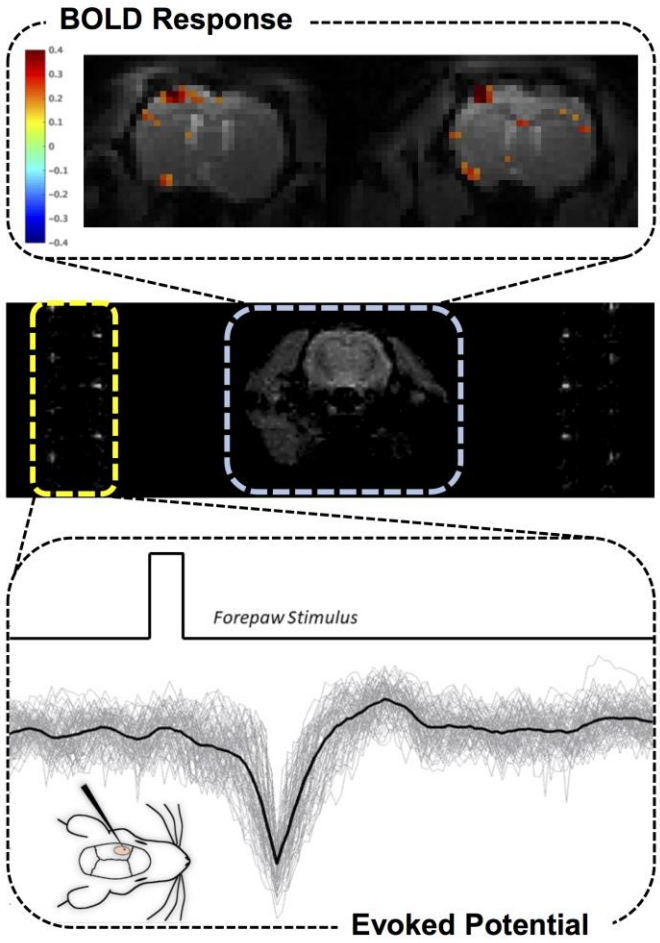

Fig. 10. Concurrent acquisition of BOLD response and evoked potential through the MR-Link Recorder system. BOLD activity correlated with stimulation trigger, show strong relationship between the BOLD response at S1FL and forepaw stimulation (Top). Simultaneously, SEP signal recorded through the electrode placed in the somatosensory cortex of the rat brain was transmitted via the MR-Link system. EP data reconstructed from fMRI image sequence show somatosensory evoked potential due to the forepaw stimulus (Bottom).

(Figure 11). Furthermore, the tSNR analysis quantitatively concluded that the wirelessly transmitted data had no deteriorating effects on the MR-image quality (Figure 11).

IV. Discussion

The MR-Link recording system utilizes the MRI scanner and its electromagnetic environment for synchronization and wireless transmission of non-MR data (Figure 2). Utilizing the inbuilt, powerful digitizer and receiver capabilities of a conventional MR-scanner, the system achieves a small form factor (20mm dia., 2gms) and requires low power to operate. As a result, the system provides an in-expensive (value/channel) and unique solution for recording various types of electrical and EP signals within MRI, while simultaneous imaging. The gradient synchronized, variable-gain amplifier provides gradient artifact free data that is digitized and communicated back to the MR-system, thus achieving micro-second scale synchronization.

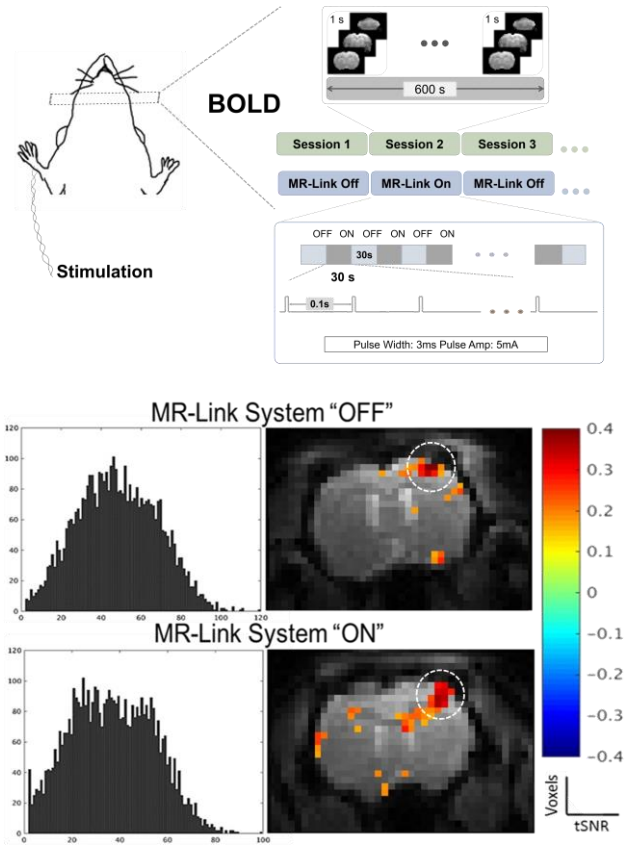

Fig. 11. MR-compatibility study using an in vivo experimental paradigm (top): BOLD images were acquired while the rat was administered forepaw stimulation with parameters shown on top. The BOLD response was recorded from rat brain for two sets of experimental conditions. One condition included the MR-Link system operating normally ("ON") and wirelessly transmitting EP data to scanner receiver coil. In the second condition, the MR-Link system was disconnected from its power supply and kept in the "OFF" state. BOLD response and tSNR comparison of the MRI image for the discussed conditions are shown(bottom).

A. Utilizing MR-hardware for EP data recording

The current implementation of the method only shows recording through a single channel and overlays the data on MR-images, but similar technique can be used to record multi-channel EP signals. For multichannel operation, each channel's carrier frequency can be separated out into non-overlapping bands. The study configuration (receiver bandwidth: 333KHz and transmission channel bandwidth: 19.2KHz) allows for simultaneous recording of 9 electrophysiological channels. Moreover, additional recording channels can be incorporated by extending the receiver bandwidth and/or the FOV along the readout direction without compromising repetition time (TR).

A sampling rate of 1.3KHz, achieved during functional imaging was sufficient for slow varying EP signals (ECG, EEG, LFP etc.). The sampling rate was limited by the duration between each readout trains, as RF excitation, slice selection and crusher gradients were applied during this time and no usable data could be gathered. This 'blip' period was minimized (~5ms) through the design of the MR-pulse sequence.

Furthermore, application specific design of the transmitting unit and data compression makes it possible to increase the number of simultaneous recording channels significantly [26]. The MR-scanner system works as a high frequency mixer and converts the transmission frequency at some intermediate frequency with respect to the scanner center frequency and digitizes the signal at a high sampling rate (Figure 6). Several different forms of processing algorithm can subsequently be implemented on the digitized data which is made available through the custom-built software. Thus, any combination of time division multiplexing (TDM) or frequency division multiplexing (FDM) transmission methods can be utilized to accommodate higher number of channels at increased data rate.

The data extraction algorithm worked consistently (data not shown) as the transmission channel was placed at different distances with respect to the MR-scanner center frequency. The digital modulation method (FSK) was comparatively better immune to noise and amplitude fluctuations and did not require any additional dedicated calibration signal, as shown in the implementation by Hanson et al [24]. Individual frequency channels were well separated and detectable at very low transmission power levels. Furthermore, the simple nature of the processing algorithm may facilitate real-time monitoring of the EP data during simultaneous imaging through integration of the custom software with the imaging platform.

Another interesting application of the method can be found with the availability of dual-tuned receiver coils. The Non-MR data can be transmitted at a 'X'-nuclear coil frequency with continuous proton imaging. Current implementation allows the MR-Link system to send the wireless data at a large range of frequencies from 75MHz to 1GHz. This can eliminate the systems dependency on a specific pulse sequence (EPI) as the EP data can be continuously monitored through accessing the 'X'-nuclear coil data. Additionally, the EP signals can be recorded within the MR-Link hardware and transmitted in bursts after each imaging cycle. These bursts can be picked up by MR-receiver coil through a custom designed short duration MR-pulse sequence.

B. Power harvesting opportunities

Powering the recording system within the MR-environment requires significant attention since additional powering circuitry can affect the operation of the MR-scanner. The low-powered, battery operated recording and transmission system presented in the study is well suited to be powered through a variety of different approaches. An attractive method which is currently being explored is wirelessly powering the device by harvesting energy from the strong magnetic flux generated by the MRI [27]. Wireless powering removes cables running through the MRI bore, improve the functionality of the device as well as the MRI. The advantages of wireless powering provide a strong case for its implementation into the MR-Link device to further make it into a stand-alone system.

C. Gradient artifact-free EP data extraction

The various studies in this project were conducted with the MRI scanner operating at its maximum gradient slew rate of 200mT/m. The gradient and RF artifacts were minimized through the variable sensitivity amplifiers and the selective sampling algorithm. Furthermore, the moving average filter implemented on the µC attenuated any leakage artifacts. This averaging scheme combined with a synchronized sampling method allowed the MR-Link system to completely remove any gradient artifacts from the data before transmission. Thus, the

extracted data from the MR-image did not require any additional retrospective digital processing[20].

The MR-Link system provides a simple and effective solution for high fidelity neural recording in simultaneous fMRI studies by utilizing MR-surplus hardware. Gradient triggered sampling and discrete time variable sensitivity amplifier combined with wireless reception of electrophysiological signal by MR coil address technical challenges regarding the signal integrity and electromagnetic artifacts, while reducing the overall complexity by removing the dependence on bulky synchronization and shielding systems. Additionally, further refinement and implementation of the system will be focused on future human applications. Therefore, the success of the current research is expected to open new avenues for widely accessible and integrative neuroimaging tools.

REFERENCES

[1] P. A. Valdes-Sosa *et al.*, "Model driven EEG/fMRI fusion of brain oscillations," *Human Brain Mapping*, vol. 30, no. 9. pp. 2701–2721, 2009.

[2] R. Goebel and F. Esposito, "The added value of EEG-fMRI in imaging neuroscience," in *EEG - fMRI: Physiological Basis, Technique, and Applications*, 2010, pp. 97–112.

[3] P. Ritter and A. Villringer, "Simultaneous EEG-fMRI," *Neuroscience and Biobehavioral Reviews*, vol. 30, no. 6. pp. 823–838, 2006.

[4] S. Debener, M. Ullsperger, M. Siegel, and A. K. Engel, "Single-trial EEG-fMRI reveals the dynamics of cognitive function," *Trends Cogn. Sci.*, vol. 10, no. 12, pp. 558–563, 2006.

[5] E. K. Miller *et al.*, "What we can do and what we cannot do with fMRI.," *Annu. Rev. Neurosci.*, vol. 24, no. 7197, pp. 869–878, 2008.

[6] J. Jorge *et al*., "Simultaneous EEG-fMRI at ultra-high field: Artifact prevention and safety assessment," *Neuroimage*, vol. 105, pp. 132–144, 2015.

[7] K. J. Mullinger, P. Castellone, and R. Bowtell, "Best Current Practice for Obtaining High Quality EEG Data During Simultaneous fMRI," *J. Vis. Exp.*, no. 76, p. 50283, 2013.

[8] B. He and Z. Liu, "Multimodal functional neuroimaging: integrating functional MRI and EEG/MEG.," *IEEE Rev. Biomed. Eng.*, vol. 1, pp. 23–40, 2008.

[9] R. J. Huster, S. Debener, T. Eichele, and C. S. Herrmann, "Methods for simultaneous EEG-fMRI: an introductory review.," *J. Neurosci.*, vol. 32, no. 18, pp. 6053–60, 2012.

[10] J. Gotman, E. Kobayashi, A. P. Bagshaw, C. G. Bénar, and F. Dubeau, "Combining EEG and fMRI: A multimodal tool for epilepsy research," *Journal of Magnetic Resonance Imaging*, vol. 23, no. 6. pp. 906–920, 2006.

[11] Z. Liu, J. a de Zwart, C. Chang, Q. Duan, P. Van Gelderen, and J. H. Duyn, "Neuroelectrical Decomposition of Spontaneous Brain Activity Measured with Functional Magnetic Resonance Imaging," *Cereb. Cortex*, no. November, pp. 3080–3089, 2013.

[12] P. J. Allen, G. Polizzi, K. Krakow, D. R. Fish, and L. Lemieux, "Identification of EEG events in the MR scanner: the problem of pulse artifact and a method for its subtraction.," *Neuroimage*, vol. 8, no. 3, pp. 229–239, 1998.

[13] K. Anami *et al.*, "Stepping stone sampling for retrieving artifact-free electroencephalogram during functional magnetic resonance imaging," *Neuroimage*, vol. 19, no. 2, pp. 281–295, 2003.

[14] Z. T. H. Tse *et al.*, "A 1.5T MRI-conditional 12-lead electrocardiogram for MRI and intra-MR intervention," *Magn. Reson. Med.*, vol. 71, no. 3, pp. 1336–1347, 2014.

[15] S. Assecondi, C. Lavallee, P. Ferrari, and J. Jovicich, "Length matters: Improved high field EEG-fMRI recordings using shorter EEG cables," *J. Neurosci. Methods*, vol. 269, pp. 74–87, 2016.

[16] P. J. Allen, O. Josephs, and R. Turner, "A method for removing imaging artifact from continuous EEG recorded during functional MRI.," *Neuroimage*, vol. 12, no. 2, pp. 230–9, 2000.

[17] R. I. Goldman, J. M. Stern, J. Engel, and M. S. Cohen, "Simultaneous EEG and fMRI of the alpha rhythm.," *Neuroreport*, vol. 13, no. 18, pp. 2487–92, 2002.

[18] J. R. Ives, S. Warach, F. Schmitt, R. R. Edelman, and D. L. Schomer, "Monitoring the patient's EEG during echo planar MRI," *Electroencephalogr. Clin. Neurophysiol.*, vol. 87, no. 6, pp. 417–420, 1993.

[19] M. E. H. Chowdhury, K. J. Mullinger, P. Glover, and R. Bowtell, "Reference layer artefact subtraction (RLAS): A novel method of minimizing EEG artefacts during simultaneous fMRI," *Neuroimage*, vol. 84, pp. 307–319, 2014.

[20] Z. Liu, J. A. de Zwart, P. van Gelderen, L. W. Kuo, and J. H. Duyn, "Statistical feature extraction for artifact removal from concurrent fMRI-EEG recordings," *Neuroimage*, vol. 59, no. 3, pp. 2073–2087, 2012.

[21] R. K. Niazy, C. F. Beckmann, G. D. Iannetti, J. M. Brady, and S. M. Smith, "Removal of FMRI environment artifacts from EEG data using optimal basis sets," *Neuroimage*, vol. 28, no. 3, pp. 720–737, 2005.

[22] H. Xia, D. Ruan, and M. S. Cohen, "Removing ballistocardiogram (BCG) artifact from full-scalp EEG acquired inside the MR scanner with Orthogonal Matching Pursuit (OMP)," *Front. Neurosci.*, no. 8 JUL, 2014.

[23] Q. Luo, X. Huang, and G. H. Glover, "Ballistocardiogram artifact removal with a reference layer and standard EEG cap," *J. Neurosci. Methods*, vol. 233, pp. 137–149, 2014.

[24] L. G. Hanson, T. E. Lund, and C. G. Hanson, "Encoding of electrophysiology and other signals in MR images," *J. Magn. Reson. Imaging*, vol. 25, no. 5, pp. 1059–1066, 2007.

[25] B. Weissler *et al.*, "PET/MR synchronization by detection of switching gradients," *IEEE Trans. Nucl. Sci.*, vol. 62, no. 3, pp. 650–657, 2015.

[26] K. H. Teng, T. Wu, X. Liu, Z. Yang, and C. H. Heng, "A 400 MHz Wireless Neural Signal Processing IC with 625 × On-Chip Data Reduction and Reconfigurable BFSK/QPSK Transmitter Based on Sequential Injection Locking," IEEE Trans. Biomed. Circuits Syst., vol. 11, no. 3, pp. 547–557, 2017.

[27] J. Höfflin, E. Fischer, J. Hennig, and J. G. Korvink, "Energy Harvesting with a figure-8 coil - towards energy autonomous MRI detection," no. April 2013, 2016.